Machine Learning Aided Automated Design for Reliability of Power Electronic Systems

Tomislav Dragičević, *Senior Member, IEEE*, Patrick Wheeler, *Senior Member, IEEE*, and Frede Blaabjerg, *Fellow, IEEE*

Abstract

This paper proposes a new machine learning aided methodology for automated design of power electronic systems that embeds the reliability engineering within the design process. In sharp contrast to state of the art design approaches that either do not consider the system's reliability as a performance metric or are limited only to reliability evaluation for a certain fixed set of design parameters, the proposed method establishes functional relationships between design parameters and reliability metrics, and uses them as the basis for optimal design. The first step in this new framework is to create a surrogate model of the power converter that can quickly map the variables characterizing the operating conditions (e.g. ambient temperature, irradiation) and design parameters (e.g. switching frequency, dc link voltage) into variables characterizing the thermal stress of a converter (e.g. mean temperature and temperature variation of its devices). This step is carried out by training a dedicated artificial neural network (ANN) using either the experimental or simulation data. The resulting network can be named as ANN_1 and deployed as an accurate and extremely fast surrogate converter model to evaluate its lifetime consumption (LC) in a yearly mission profile for a large set of design parameter values. The resulting data is then used to train ANN_2, which becomes a function that explicitly maps the design parameters into a yearly LC. To verify the proposed methodology, ANN_2 is finally deployed in conjunction with the standard converter design tools on an exemplary grid-connected PV converter case study to find the optimal balance between the reliability and output filter size in the system.

Index Terms

Automated design for reliability (ADfR), machine learning, power electronic systems.

I. Introduction

The use of power electronic converters has become omnipresent nowadays. They are the key enablers of technologies such as renewable energy systems, electrical vehicles and their charging

infrastructure, variable speed drives, as well as uninterruptible power supply (UPS) systems and microgrids [1], [2]. Much like any other system, power converters are prone to failures. Such failures cause downtimes that often require costly maintenance procedures, especially if the power electronic system is located in the remote or offshore location. Moreover, such failures may also have catastrophic consequences in mission critical applications or significantly reduce the energy yield of renewable energy systems [3].

Redundancy is one of the most attractive approaches to provide the failure-tolerant capability to power electronic systems. While being highly effective in this regard, redundant design will normally significantly increase the cost and size of the system, thus compromising its competitiveness in the market. Another scheme is to select the individual components in the converter (e.g. switching devices, inductors, capacitors) with sufficient thermal and electrical stress margin, thus expecting their low failure rates and, consequently, high reliability of the overall system. However, with this approach, the quantitative reliability metrics of individual devices are not taken into account, and for this reason it is also not possible to automatically design the system for specified reliability.

To circumvent the drawbacks of aforementioned methods, the research in reliability of power electronic systems has recently experienced a paradigm shift towards the so called design for reliability (DfR) approach [4], [5]. The main idea here is to deploy the detailed reliability models of individual components and use them to calculate a concrete numerical metric that quantifies the reliability of the whole system. Since the most vulnerable part of the converter are semiconductor devices, the research focus in the DfR area has mostly been on investigating the impacts of mission profiles (e.g. ambient temperature and power processed by the converter over a certain time period) on the thermal loading (i.e. the junction temperature) of power devices, which has a direct influence on their lifetime consumption (LC). Assuming that all other components in the system are significantly more reliable, the LC of power devices is hence normally considered as the representation of the whole system's LC [6]–[9]. It is also possible to combine LCs of several components in the system to assess the system level reliability [10].

Nevertheless, the LC estimates in all of the DfR approaches mentioned above are made on power electronic systems whose design parameters are already fixed and hence no explicit inverse relationship between the yearly LC and design parameters can be established in this way. Due to this limitation, the system designer will generally need to evaluate numerous combinations of design parameters via a time-consuming trial and error to get an idea about how they affect the

LC, and select the suitable design correspondingly.

The aim of this paper is to bridge this knowledge gap by building upon the principal DfR concepts in order to develop a fully automated design for reliability (ADfR) tool. The key enabling methodology for this development is machine learning, and more particularly the artificial neural networks (ANNs). It is well known that ANNs are universal function approximators, i.e. they can approximate any given input/output data relationship with arbitrary precision [11]. Here, we take advantage of this capability for two different purposes. First, we use it build a surrogate model of the power converter that is able to estimate the thermal stress of any device in the converter as a function of design parameters and the mission profile several orders of magnitude faster compared to running the detailed simulation model. Such a surrogate model, labeled as ANN_1, has similar functionality as a lookup table reported in e.g. [9], but consumes significantly lower amount of memory, thus allowing to embed any design parameter as an input to the model. In addition, it has much better capability to generalize nonlinear input/output data relationship, thereby providing more precise estimates of the junction temperatures. The second purpose of ANN is to establish the functional relationship between design parameters and yearly LC in a network labeled ANN_2. Again, this process resembles the ones presented in [7]–[9], but here the LC evaluation is systematically repeated for a large number of design parameter variations to generate the training data for ANN_2 which, after training, gives an explicit functional relationship between design parameters and LC, thus providing a key basis for ADfR. ANN_2 can consequently be used either individually or in conjunction with other design tools, e.g. if it is desirable to balance the reliability of the system with other metrics such as cost, weight/volume, or others.

The rest of the paper is organized as follows. Section II describes the power electronic system under consideration, i.e. the single-phase grid-connected H-bridge PV inverter, although the proposed methodology is generic and thus applicable to any other converter topology. In Section III, the conventional system design and reliability evaluation methodologies are briefly revised, while Section IV provides the background about the artificial neural networks (ANNs). In Section V, the proposed design procedure is described step by step. The procedure is then verified in Section VI, where switching frequency and dc-link voltage reference of the grid connected PV inverter that provide the optimal balance between the reliability and size of the system, are found via proposed approach. Finally, the conclusion of the paper is given in Section VII.

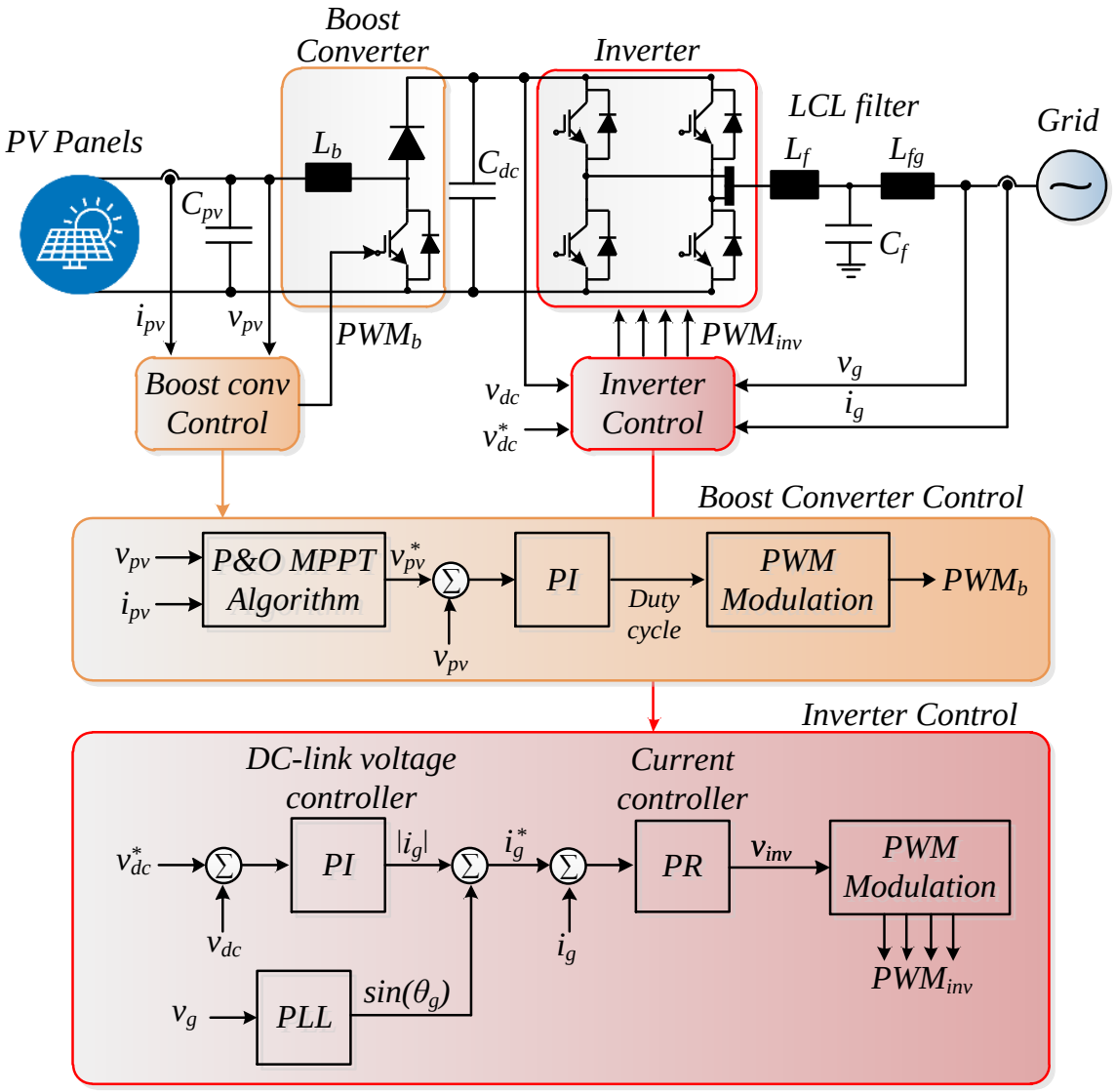

Fig. 1. System configuration and control structure of a two-stage single phase grid-connected PV system. Here, PI is proportional-integral, PR is proportional-resonant, PLL is phase locked loop, PWM is pulse width modulator.

II. Description of the Case Study

A. System Description

The design methodology proposed in this paper is verified on a power electronic system case study that involves a two-stage grid connected single-phase PV inverter with rated power of 10 kW, as shown in Fig. 1. The system comprises a dc-dc boost converter, which operates the maximum power point tracking (MPPT) algorithm and a full-bridge dc-ac converter that regulates the intermediate dc link voltage v_{dc} and grid side current using cascaded linear control loops.

The correct angle for the current controller is provided by a phase-locked loop (PLL).

Table I indicates the design parameters of the system. These parameters have a strong influence on its performance, size/cost and reliability, and should therefore be carefully selected. In a case study analyzed in this paper, some of the listed parameters are considered to be fixed while others are designable. For instance, the switching frequency of the inverter f_{sw}, reference dc link voltage v_{dc}^{*}, and LCL filter parameters (L_f, C_f, L_{fg}) are chosen as designable parameters. By looking at the relationships between these parameters, it is intuitively clear that higher f_{sw} will yield a lower switching ripple, thus permitting the usage of a smaller filter. However, higher switching frequency will also result in higher switching losses, thereby causing larger junction temperatures of the power devices and shortening their lifetime.

While the aforementioned design trade-off between the reliability and size of the system is well-known, the existing research works fail to establish explicit relationships between these two metrics and to embed them as a part of the design process. More particularly, the works labeled under the *Design for Reliability* alias (e.g. [8], [9]) assume predetermined design and only provide lifetime prediction for a given design and mission profile. Therefore, it would be more appropriate to label the methods proposed in these works as reliability evaluation methods. On the other hand, the works that consider optimal design of power electronic systems (e.g. [12], [13]) do not take into account the reliability of the system as a performance metric. The aim in this paper is to fill this knowledge gap by providing a holistic design methodology that simultaneously takes into account the performance, reliability and size/cost of the system.

B. Mission Profile

Besides the design parameters, the mission profile in which the power converter is operated has a notable impact on the junction temperatures of power devices. Mission profile characterizes the operating conditions such as the ambient temperature and the power processed by the converter. As shown in [9], mission profiles can vary significantly according to geographic location.

In this paper, a yearly mission profile recorded in Aalborg, Denmark has been used for the considered case study, as shown in Fig. 2. It can be seen from the figure that the profile involves yearly irradiation and ambient temperature data. Depending on the particular PV panel characteristics, which can be found in the manufacturer data-sheet, such data can easily be translated into the power processed by the inverter P_{in}, assuming that the maximum possible

TABLE I

PARAMETERS OF THE TWO-STAGE SINGLE PHASE PV SYSTEM (FIG. 1)

Fixed parameters	
PV inverter rated power	10 kW
Boost converter inductor	L_b = 1.8 mH
PV-side capacitor	C_{pv} = 1000 μF
Dc-link capacitor	C_{dc} = 1100 μF
Grid nominal frequency	$\omega_g = 2\pi \times 50 rad/s$
Grid nominal voltage (RMS)	230 V
Designable parameters	
Inverter LCL filter	L_f, C_f, L_{fg}
Inverter switching frequency	f_{sw}
Dc-link voltage reference	v^*_{dc}

power is always extracted. P_{in} and T_a can then be used for obtaining the junction temperatures from the detailed simulation model, as detailed in Section III-B.

III. RELIABILITY OF THE POWER ELECTRONIC SYSTEM

In principle, the reliability of power electronic system can be improved in the following three ways [4]: 1) by selecting a suitable topology of the converter, i.e. the one that either minimizes the number of components or that provides redundancy in case of failures 2) by choosing high quality individual components in the system that are less likely to fail, and 3) by reducing the stress level of the components [4].

A. Design Trade-Off

In this paper, it is assumed that the circuit topology of the converter is fixed and that the type of components most prone to failures, i.e. the switching devices, are preselected. To this end, the main design goal from a reliability point of view is to minimize the stress level on the switching devices. As mentioned before, lower f_{sw} leads to lower switching loss, which in turn induces lower temperature swings and hence leads to longer lifetime for the devices. However, lower f_{sw} also results in higher harmonic distortion and in a slower dynamic response of the converter, while it also requires bulkier and more expensive passive filters. Similarly, higher

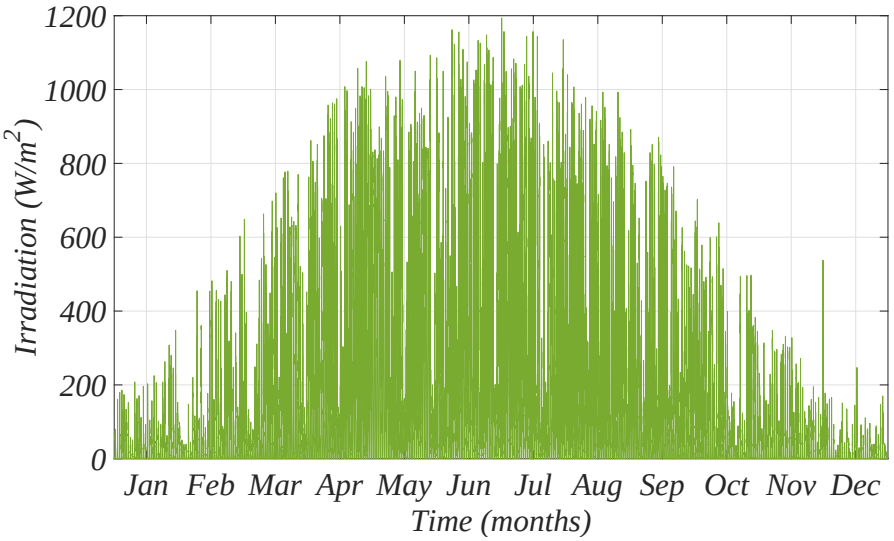

(a) Solar irradiation.

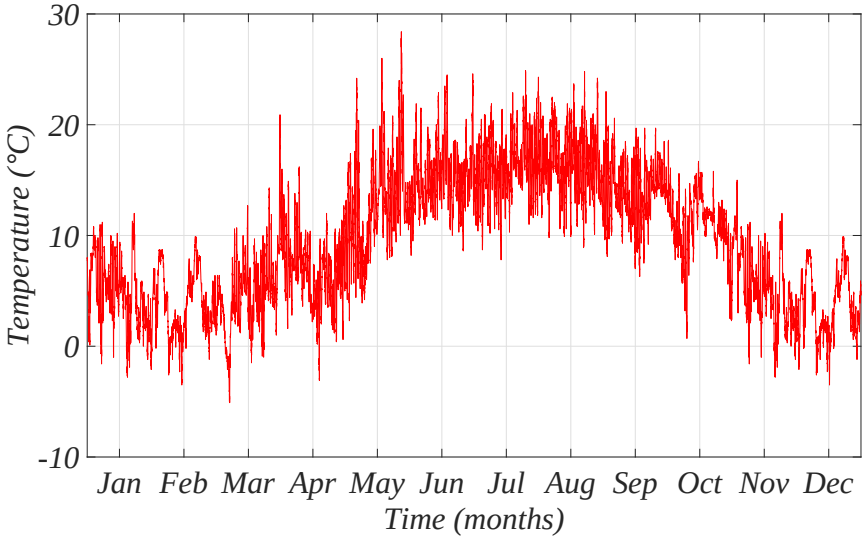

(b) Ambient Temperature.

Fig. 2. Yearly mission profile from the PV installation site in Aalborg, Denmark with a sampling rate of 1 min/sample.

v_{dc} increases the switching losses and causes higher switching ripple [14], but the higher it is, the more control bandwidth it provides [15]. In this respect, it is clear that f_{sw} and v_{dc} are two key design parameters that affect the reliability, performance and size (cost) of the system. Therefore, these two parameters should be explicitly selected to yield the best balance between these metrics.

TABLE II

PARAMETERS OF THE LIFETIME MODEL OF AN IGBT MODULE

A	3.4368×10^{14}
α	-4.923
β_0	1.942
β_1	$-9.012x10^{-3}$
C	1.434
γ	-1.208
f_d	0.6204
ar	0.28
E_a	0.06606 eV
k_B	$8.6173324 \times 10^{-5} eV/K$

In order to provide a framework for truly optimal design, the well-known conventional design procedure (as in e.g. [12] and [14]) is here combined with the LC of the system, which can be considered as its reliability metric. The methodology for evaluating the LC of power devices is described in the following subsection.

B. Lifetime Evaluation Procedure

It is well known that the power devices are the most vulnerable components of power electronic converters. Depending on the mission profile (T_a and P_{in}) and design parameters (v_{dc}, f_{sw}, heat sink parameters and others), these devices will experience junction temperature swings that cause their wear-out. The temperature swings occur due to changing switching and conduction losses caused both by the varying loading (mission profile) and the sinusoidal shape of the inverter current. For a given operating condition, the thermal stress on the device can be characterized by the mean temperature value T_{jm}, the amplitude of oscillation ΔT_j and the period of oscillation t_{on}.

The concrete values of T_{jm}, ΔT_j and t_{on} can be extracted from the detailed simulation model of the converter and its associated thermal network. However, it is unfeasible to run the detailed simulation for the whole yearly mission profile period. For this reason, an approximate model of the converter that can quickly translate the mission profile and design parameters into junction

temperatures, is commonly developed. The development of such model using machine learning methodology is described in the following section.

For numerous types of devices, empirical models that quantify the effect of each cycle on the lifetime of the device have been constructed based on experimental data. An example of one such model is given in [16]:

$$\begin{aligned} N_f =& A \times (\Delta T_j)^{\alpha} \times (ar)^{\beta_1 \Delta T_j + \beta_0} \times \left[\frac{C + (t_{on})^{\gamma}}{C+1} \right] \\ & \times exp\left(\frac{E_a}{k_b \times T_{jm}} \right) \times f_d, \end{aligned} \tag{1}$$

where N_f is the number of cycles that a device can tolerate before failure if stressed with a certain ΔT_j, T_{jm} and t_{on}. The other parameters required to evaluate (1) can be obtained experimentally. An exemplary set of parameters is taken from [16] and it is shown in Table II.

The inverse of N_f indicates the level of damage that a device sustains under certain stress conditions. In line with this, the total LC over a certain period can then be estimated using the Miner's rule as follows:

$$LC = \sum \frac{n_i}{N_{fi}} \tag{2}$$

where n_i is the number of cycles that result in incremental damage $1/N_{fi}$. Therefore, in order to find out the total LC that occurs over a certain time period, it is necessary to count the total number of temperature cycles and associate each cycle with a corresponding N_{fi}.

For a grid-connected PV system, two basic types of junction temperature cycles can be identified. The first type of cycles is caused by the mission profile and they are normally extracted from the yearly junction temperature data using the rain-flow counting algorithm. Such an algorithm extracts all the cycles and associates each one of them with a specific ΔT_j, T_{jm} and t_{on}, thus enabling the usage of (1). The second type is a repercussion of injecting the sinusoidal current at fundamental frequency into the grid. Therefore, this type has a fixed period t_{on}, while given ΔT_j and T_{jm} can be extracted from the converter model and the rain-flow counting data, respectively. Therefore, the total LC can be calculated by adding the two contributions. It should also be noted that the parameters in (1) are usually not deterministic and can vary within certain ranges. If these effects are taken into account, the overall LC is normally evaluated using the Monte-Carlo analysis and represented as the probability distribution function [17]. However, the consideration of the parameter variations in (1) is out of the scope of this paper, and will be considered in the future work.

IV. ANN BASED MODELING

A. Motivation for Using the ANNs

As explained in the previous section, it is essential to establish a simple model of the converter that would be able to translate the yearly mission profile data into a yearly junction temperature variation. The state of the art approaches deal with this task by simulating the detailed model of the converter with associated thermal network for several selected combinations of P_{in} and T_a and extracting the corresponding ΔT_j and T_{jm}. These data are then fed to the look-up table (LUT) that serves as a surrogate model of the converter.

However, there are are several fundamental limitations associated with this approach. First, LUTs are not suitable for high-dimensional data mapping since they suffer from the inefficient use of memory space. This is particularly restricting if one would seek to construct a more complicated surrogate model of the power electronic system where it would be required to map both the mission profile and design parameters to the junction temperatures. Secondly, LUTs are unable to learn general nonlinear relationships between the input data and output data since they are based on linear interpolation. While the second issue could be improved by using more data points, this would not be feasible in high-dimensional spaces due to limited memory. For these reasons, LUTs have been only used to map mission profile data (i.e. P_{in} and T_a) to junction temperatures, assuming that all other design parameters are fixed [9].

In order to come around this difficulty, in this paper we propose the usage of a forward artificial neural network (ANN) to serve as a more fast, accurate and flexible surrogate model of the converter. It has been shown in [11] that forward ANN is a universal function approximator, i.e. that the parameters in its structure can be adjusted in such a way to approximate any given input/output data relationship with arbitrary precision, given that the network is sufficiently large.

The key advantage of using ANN over LUT is that ANN is only trained on the input data, and the number of training parameters will generally be several orders of magnitude lower than the number of data points. For this reason, ANN has much lower memory requirements than LUT. Moreover, ANN can be trained to explicitly map the influence of mission profiles and any design parameters (e.g. v_{dc}^{*} and f_{sw}) on the junction temperature of the devices, with arbitrary precision, even if these relationships are highly nonlinear. The following subsection provides a basic theoretical introduction to ANNs.

B. ANN Principle

Numerous types of ANNs have been proposed in the literature [18]. Particular network choice depends mostly on the nature of relationships between inputs and outputs in the data. When outputs depend on historical values of the inputs and outputs, recurrent neural networks are the most suitable. In the case study of this paper, the relationship between design parameters and mission profiles with the junction temperatures is static. For this reason, forward ANN has been selected for the case-study here. Forward ANNs are the most commonly used machine learning algorithms and have been applied already to various electrical engineering problems, from predicting the voltage voltage distortion in electrical distribution networks [19], to designing the microwave filters [20], [21].

A forward ANN comprises an input layer, one or more hidden layers, and an output layer. Each of these layers comprises a number of neurons that process the information coming from neurons in the layer below. To calculate the output of a certain neuron γ_i^l in layer l, the outputs of all the neurons z_j^{l-1} ($j = [1..N_{l-1}]$) in the layer below $l-1$ are multiplied with given weights ω_{ij}^l and the bias term b_i^l is then added. The result is processed through an activation function σ that usually takes the form of a sigmoid function, i.e. $\sigma(\gamma) = 1/(1+e^{-\gamma})$, to generate the output z_i^l. This output then becomes one of the inputs for the layer above, $l+1$, and the same procedure is repeated to calculate the output of other neurons in layer l.

In the input layer, z_i^1 takes the form of inputs. On the other hand, the output layer typically uses the linear activation function to allow any numerical value, as opposed to being limited to [0,1] range as the sigmoid function. To sum up, the complete signal flow of the ANN can be described as follows:

- Layer 1 (input):

$$z_i^1 = x_i \quad i = 1, .., N_1 \tag{3}$$

  where x_i are the inputs.

- Layers l = 2,..,$L-1$ (hidden):

$$z_i^l = \sigma\left(\sum_{j=1}^{N_{l-1}} w_{ij}^l z_j^{l-1} + b_i^l\right) \quad i = 1, .., N_l. \tag{4}$$

- Layer L (output):

$$y_i = w_i^L z_i^L \quad i = 1, .., N_L \tag{5}$$

  where y_i are the outputs.

It has been shown in [11] that forward ANN is an universal function approximator, i.e. that the weights and bias terms in its structure can be adjusted so as to approximate any input/output data relationships with arbitrary precision. These parameters are adjusted during the training process, normally using the back-propagation algorithm. This algorithm takes advantage of the continuous differentiability of the ANN to find out the direction in which the w_{ij}^{l} and b_{i}^{l} parameters should be adjusted in each training iteration to reduce the error between the measured output data and prediction made by the ANN from previous iterations [22]. Back-propagation is a well known algorithm that is available in standard softwares like MATLAB.

It is important to notice that, before starting the training process, the structure of the network should be defined (i.e. the number of neurons that also determines number of weights and bias terms). To this end, if too few neurons are used, the strong nonlinear relationships may not be captured. On the other hand, over-fitting may occur in ANNs with too many neurons. However, up until now, an analytic method for selection for proper number of neurons has not been established. Therefore, they are usually selected using trial-and-error and this approach is also used in this paper.

Next subsection presents the development of two ANNs that are used in the proposed optimal design procedure, which is detailed in Section V.

C. Deployment of ANNs for Fast and Flexible LC Evaluation of the PV Inverter

This section elaborates the development of two dedicated ANNs, one that serves as a surrogate model of the converter and one that translates the design parameters into a yearly LC.

1) ANN1: Surrogate Model of the PV Inverter: The purpose of this network is to map the operating conditions and design parameters into the junction temperatures and is labeled as ANN_1. The data required to train this network is collected by running a detailed simulation model of the converter numerous times to cover some specific range of input parameter variations. After each simulation, corresponding $T_{jm,i,data}$ and $\Delta T_{j,i,data}$ are extracted. This process can be programmed to be fully automated and split on multiple PC cores, e.g. using MATLAB's Parallel Computing Toolbox. In this paper, parameter sweep with 375 simulations was carried out and all the results were obtained in approximately one hour an a workstation with 24 cores. This data set was then randomly divided into three data sets, i.e. the training set (70 $\%$ of data, corresponding to 263 data points), the validation set (15 $\%$ of data, corresponding to 56 data points) and the testing set (15 $\%$ of data, corresponding to 56 data points).

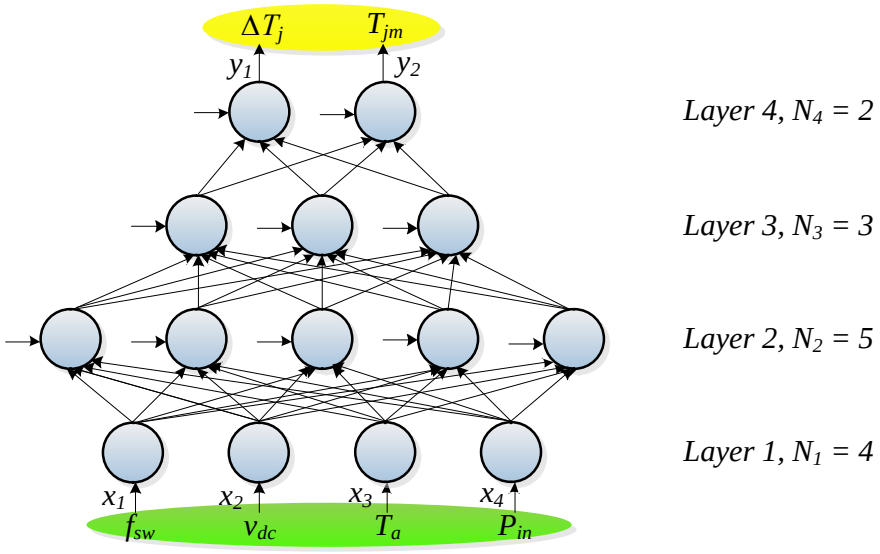

(a) Structure of the ANN_1. For simplicity, weights and bias terms are omitted from the figure. The inputs to the ANN_1 are highlighted with green color, while the outputs with yellow.

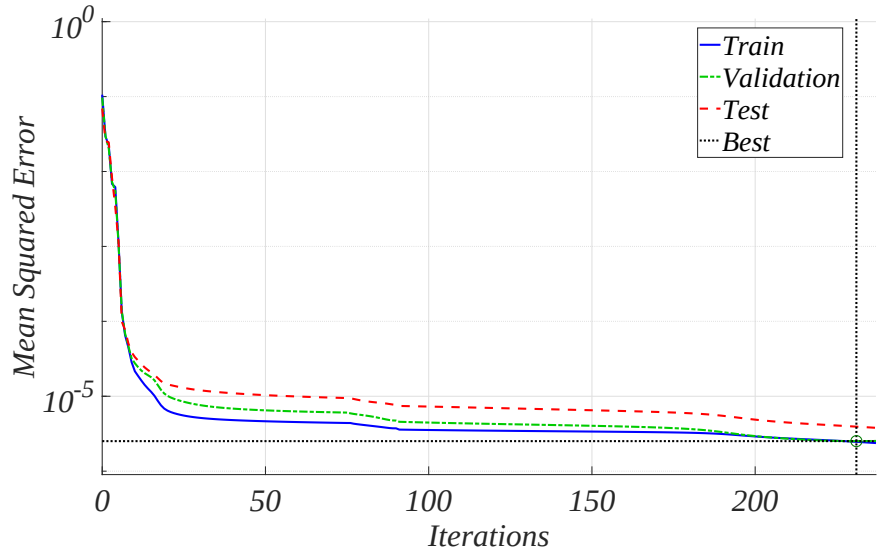

(b) Training performance of ANN_1.

Fig. 3. Artificial neural network (ANN_1) that serves as a surrogate model of the PV converter shown in Fig. 1.

Concerning the structure of the network, it has been empirically chosen to comprise an input layer, two hidden layers, and an output layer, and it is shown in Fig. 3(a). Therefore, there are 4 layers (L = 4) in total. The number of neurons in the input layer are 4 (N_1 = 4) since there are 2 design parameters v_{dc}^* and f_{sw} and two mission profile parameters, P_{in} and T_a. The number of layers in the two hidden layers are 5 and 3, respectively (N_2 = 5, N_3 = 3). Finally, the output layer comprises 2 neurons (N_4 = 2) because it is of interest to find out two values that characterize the junction temperature, i.e. its mean value T_{jm} and the amplitude of oscillation at fundamental frequency ΔT_j.

After specifying the data sets and structure of the network, ANN_1 was trained using the *train* command, which is a part of MATLAB's Machine Learning Toolbox. The improvement in the performance of ANN_1 as the training progresses, expressed as the mean squared error (MSE) between the raw data and predictions by the network for different data sets, is shown in Fig. 3(b). Extremely good matching with ultimate MSE lower than 0.00001 for all data set can be observed. Trained ANN_1 can now be used to translate the tunable design parameters and the mission profiles given in Fig. 2 into a junction temperature of the inverter's devices for any given combination of design parameters v_{dc}^* and f_{sw}. Next, ANN_1 is put to use in order to create ANN_2, as detailed below.

2) ANN2: Mapping of Design Parameters to Lifetime of the Inverter: Besides ANN_1, another network labeled as ANN_2 is trained in order to further speed up the LC evaluation procedure. This network is essentially trained to approximate the LC for a given yearly mission profile and design parameters. To this end, instead of running the rainflow counting algorithm every time when the LC estimate is needed, the LC can simply be obtained by evaluating ANN_2. The data required to train this network is collected by running the cycle counting and performing the Miner's rule on a yearly junction temperature data (obtained by evaluating ANN_1 on a yearly mission profile data) for numerous combinations of design parameters f_{sw} and v_{dc}^*. Here the f_{sw} was swept from 3 to 15 kHz with a step of 1 kHz, whereas v_{dc}^* was swept from 450 to 550 V with a step of 10 V. Consequently, the total number of data points was 143. The whole data collection process was executed in less than 25 seconds, again by using MATLAB's Parallel Computing Toolbox. As with ANN_1, this data set was randomly divided into three data sets, i.e. the training set (70 $\%$ of data, corresponding to 101 data points), the validation set (15 $\%$ of data, corresponding to 21 data points) and the testing set (15 $\%$ of data, corresponding to 21 data points).

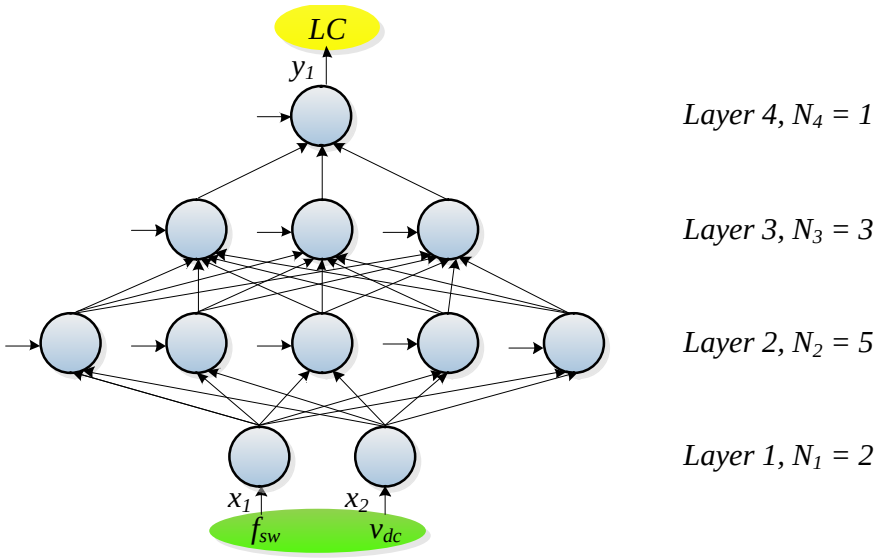

(a) Structure of the ANN_2. For simplicity, weights and bias terms are omitted from the figure. The inputs to the ANN_2 are highlighted with green color, while the outputs with yellow.

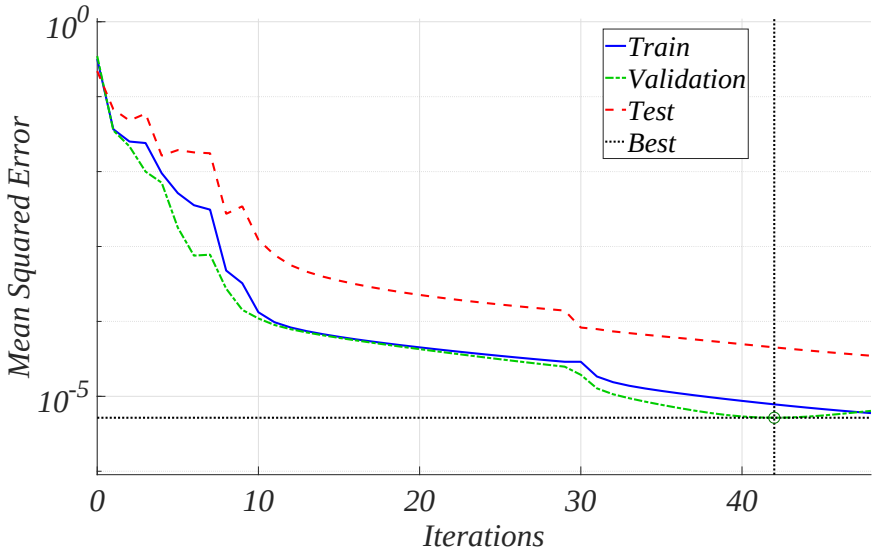

(b) Training performance of ANN_2.

Fig. 4. Artificial neural network (ANN_2) that serves as approximator of the lifetime consumption of the power electronic system.

The structure of this particular network is shown in Fig. 4(a). It is empirically selected to have an input layer, two hidden layers, and an output layer. The number of neurons in the input layer are 2 (N_1 = 2) since there are 2 design parameters v_{dc}^* and f_{sw}. The number of layers in the two hidden layers are 5 and 3, respectively (N_2 = 5, N_3 = 3). Finally, the output layer comprises 1 neuron (N_4 = 1) because our design interest is in 1 performance indicators, i.e. the converter yearly LC for a certain mission profile.

After specifying the data sets and structure of the network, ANN_2 was again trained using the *train* command. The improvement in the performance of ANN_2 as the training progresses, expressed as the mean squared error (MSE) between the raw data and predictions by the network for different data sets, is shown in Fig. 3(b). Again, very good matching with ultimate MSE lower than 0.0001 for all data set can be observed. Trained ANN_2 can now be deployed as a basis for the optimal design and combined with other designed methodologies, as described in the following section that provides the overall framework of the proposed design approach.

V. Proposed Automated Design Approach

The complete workflow of the proposed design approach is shown in Fig. 5. It can be seen that the procedure is split into a training phase that comprises 4 steps and an optimization stage with a single step. The training phase steps have been described in detail in the previous section and are only graphically summarized in Fig. 5. The ultimate result of this phase is trained ANN_2 that serves as the basis for optimal design since it can explicitly map the design parameters to yearly LC.

Nevertheless, minimization of the LC often needs to be balanced with other metrics of the system. In this paper, the idea is to optimize the trade-off between the LC and the system size, while respecting the performance metrics defined by relevant standards. To account for the power electronic system size in quantitative fashion, the standard methodology for the LCL filter design of grid-connected converters is adopted here (e.g. as suggested in [12] and [14]).

Similarly like with lifetime consumption, the required LCL filter parameters are also dependent on the f_{sw} and v_{dc}. The first step is to select the inductance of the converter side inductor L_f, which is normally done in accordance with maximum permissible ripple in the converter current, as follows [14]:

$$L_f = \frac{v_{dc}}{6 f_{sw} \Delta I_{Lmax}}. \tag{6}$$

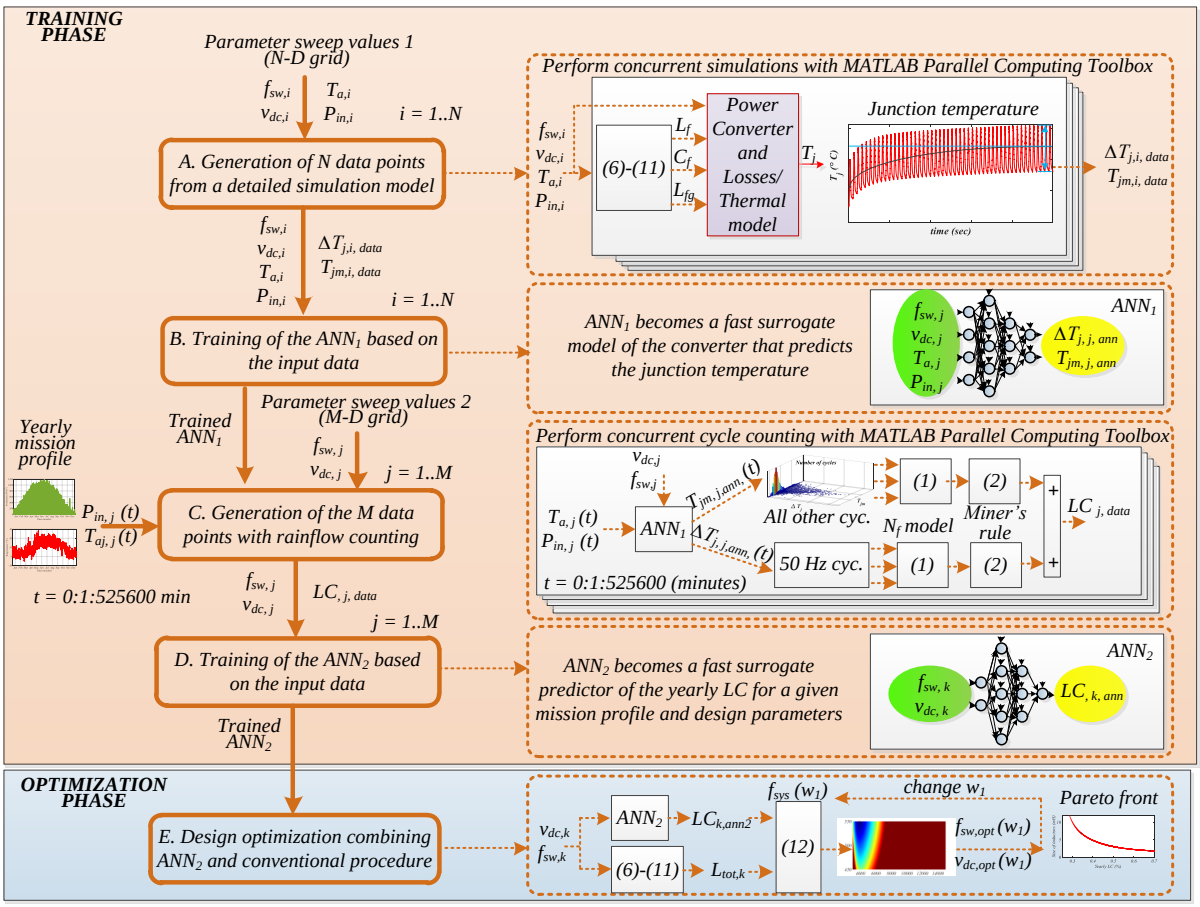

Fig. 5. Flow diagram of the proposed machine learning based design optimization of the power electronic system.

where ΔI_{Lmax} is usually selected to be 10 % of the rated converter current. The filter capacitor C_f is then selected to limit the reactive power consumption of the filter. Usually, its value is limited to 5 % of the base capacitance value, as follows:

$$C_f \leq 0.05 \cdot \frac{P_n}{\omega_g E_n^2}. \tag{7}$$

where P_n is the rated power of the converter, ω_g is the grid angular frequency, while E_n is the grid voltage amplitude. The attenuation of the harmonics from the converter side current depends also on the grid side inductor L_{fg}, as follows:

$$\frac{i_g}{i_c} = k_a = \frac{1}{1 + r(1 - L_f C_f \omega_{sw}^2)}. \tag{8}$$

where k_a is a required attenuation.

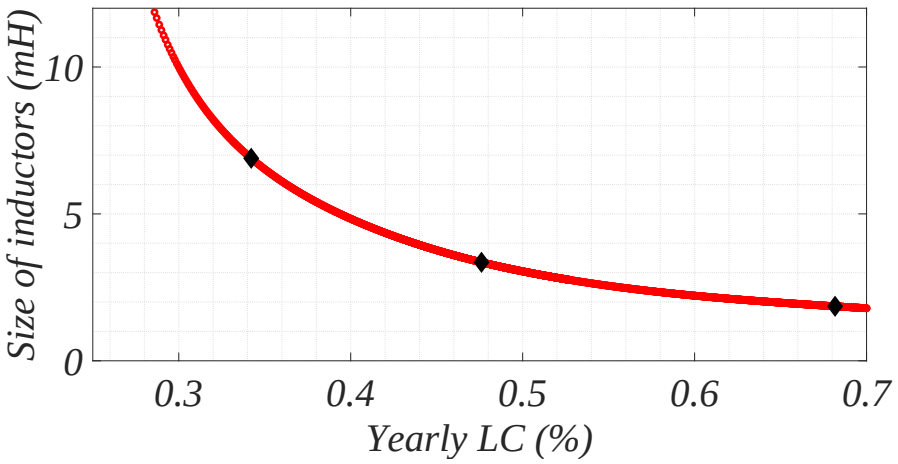

Fig. 6. Pareto front of optimal designs obtained by sweeping the parameter w_1 from (12) from 0 to 25. The three black diamonds correspond to $w_1 = 0.1$, $w_1 = 1$, and $w_1 = 10$, respectively (plots of corresponding fitness functions are shown in Figs. 7-9).

The equation (8) then provides the basis for the selection of L_{fg}:

$$L_{fg} = \frac{sqrt(1/k_a^2) + 1}{C_f \omega_{sw}}. \tag{9}$$

It can be seen from (9) that the higher the C_f, the lower L_g is needed to achieve the same level of attenuation. Therefore, it is of interest to set the C_f at the upper limit in order to reduce the size of the L_g, which has a more dominant influence on the size of the system. It is also proposed in some references to initially select C_f at a value lower than maximum in order to allow sufficient headroom for iterative re-engineering the design if the resonance frequency of the filter does not meet the following mandatory requirement [12]:

$$10 f_g < f_{res} < 0.5 f_{sw} \tag{10}$$

where

$$f_{res} = \frac{1}{2\pi} \sqrt{\frac{L_f + L_{fg} + L_g}{L_f \left(L_{fg} + L_g\right) C_f}}. \tag{11}$$

To sum up, the standard LCL filter design methods take fixed f_{sw} and v_{dc} as inputs and provide the L_f, C_f and L_{fg} as outputs using the set of equations (6)-(11). It should also be noted that (6)-(11) can be used when generating the data for training ANN_1, as indicated in Fig. 5. Considering that there is not much freedom in designing C_f, it is proposed here to use

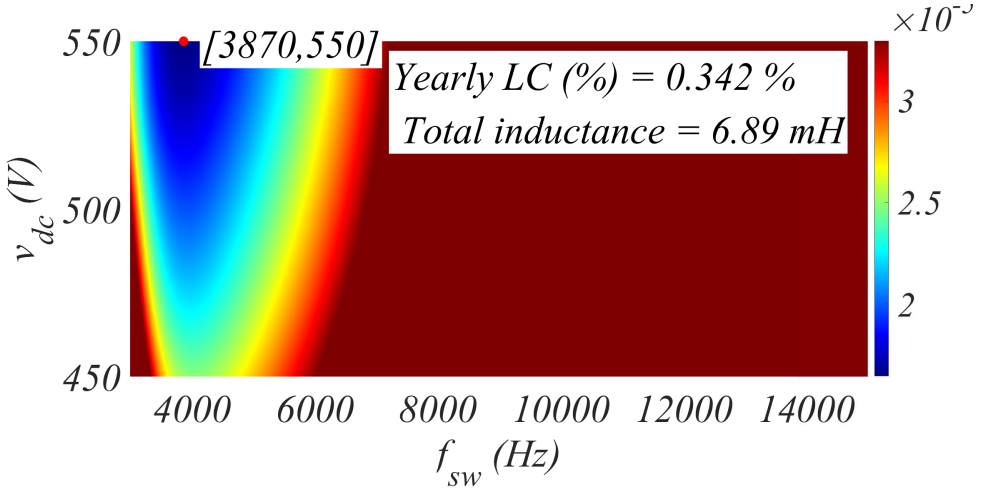

Fig. 7. Plot of the fitness function (12) for $w_1 = 0.1$. The optimum is achieved for f_{sw} = 3870 Hz and v_{dc}^* = 550 V, resulting in yearly LC of 0.342 % and L_{tot} = 6.89 mH.

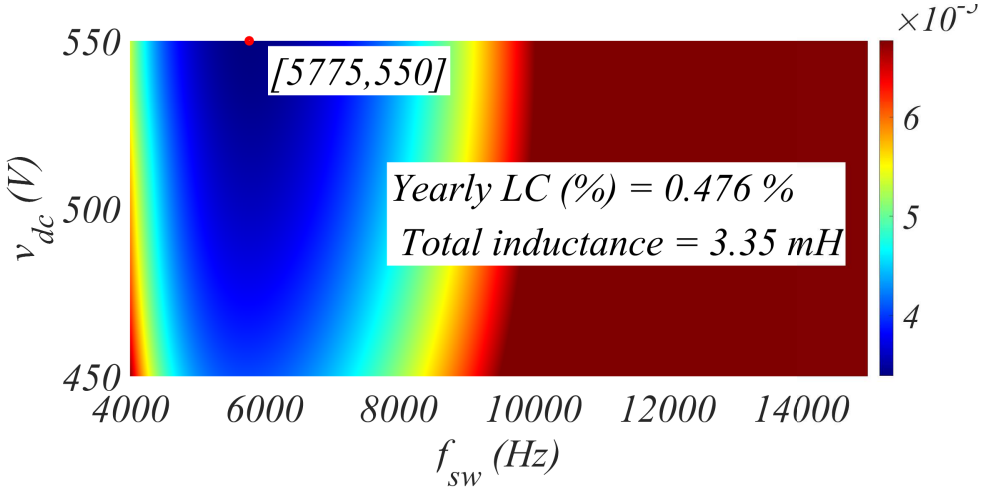

Fig. 8. Plot of the fitness function (12) for $w_1 = 1$. The optimum is achieved for f_{sw} = 5775 Hz and v_{dc}^* = 550 V, resulting in yearly LC of 0.476 % and L_{tot} = 3.35 mH.

the total size of inductors (L_{tot} = L_f+L_f) alongside with the yearly LC (predicted by ANN_2) to formulate the overall fitness function, as follows:

$$f_{sys}(w_1) = LC_{ann}^2 + w_1 \cdot (L_{tot})^2. \tag{12}$$

where w_1 is the parameter that is used to balance the importance of the two terms. By using different values of w_1, a Pareto front that characterizes the relationships between the reliability and size of the system can be constructed.

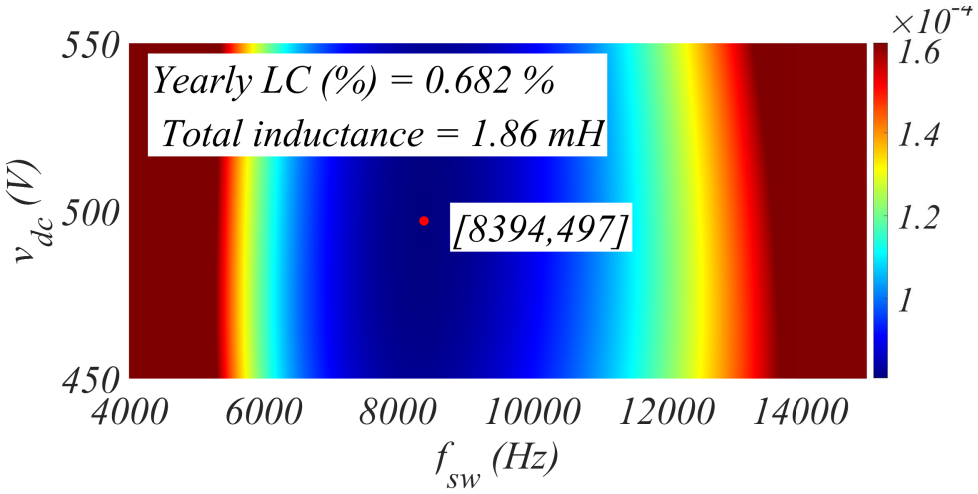

Fig. 9. Plot of the fitness function (12) for $w_1 = 10$. The optimum is achieved for f_{sw} = 8394 Hz and v^*_{dc} = 497 V, resulting in yearly LC of 0.682 % and L_{tot} = 1.86 mH.

The case-study analysis in the next chapter is carried using the fitness function (12). However, it is important to notice that this particular fitness function is only exemplary and any other one can be easily adopted within the framework of proposed design methodology. For example, it could include more metrics associated with the LCL filter design such as volume and/or losses, as in [13], or a metric that characterizes the LC of the dc link capacitor. On the other hand, more design parameters besides f_{sw} and v^*_{dc} could be considered as well, such as the parameters defining the design of the heat sink.

VI. Case Study

In order to verify the proposed design methodology, a case study for a PV system located in Denmark has been carried out. As already shown in Section II-B, irradiance and temperature data sampled minute by minute was available from a location in Aalborg/Denmark. The methodology proposed in previous section is put to use here to find the optimal trade-off between the LC and sizing of the system. Training phase was accomplished as described in Section IV, yielding a trained ANN_2 that was used in the optimization stage together with conventional design procedures to construct the corresponding Pareto front that indicates the balance between the yearly LC and the filter size. Fig. 6 shows the Pareto front obtained by sweeping the parameter w_1 from 0 to 25.

The obtained Pareto front clearly illustrates the trade-off between the yearly LC and size of the system and provides the formal framework for optimal design. As an example, three arbitrary points corresponding to three different w_1 (for w_1 = 0.1, w_1= 1 and w_1 = 10, respectively) have been selected from a given curve. The plots of associated fitness functions (together with optimal design parameters and corresponding total filter inductance, as well as LC) are given in Figs. 7, 8 and 9, respectively. It can be seen that proposed method leads to exact values of design parameters and can be used for fast optimization of power electronic systems, explicitly taking the LC of such systems as a formal performance metric.

VII. Conclusion

In this paper, a machine learning aided methodology for design optimization of power electronic systems has been proposed. The fundamental idea behind the method is to substitute the key two steps of the system's standard reliability evaluation procedure with dedicated ANNs that serve as fast and accurate approximations of these steps. As shown in Fig. 5, the first one, ANN_1, is trained to act as a surrogate model of the power electronic converter that can map the operating conditions and design parameters into junction temperature(s) of the converter's power devices. The other one, ANN_2, is trained using both ANN_1 and any given mission profile (e.g yearly) in order to accurately map the design parameters into a LC. Since both of these ANNs can be evaluated several orders of magnitude faster than standard steps, numerous design parameter combinations can be tested almost instantaneously in order to shed light on their influence of design goals. Here, this capability was exploited in order to formally investigate the influence of two exemplary design parameters, i.e. f_{sw} and v_{dc}^* on the trade-off between the size of the filter in the single-phase grid-connected PV system and the LC of the devices in the converter. With aid of proposed methodology, this trade-off was represented with the Pareto curve that provides the precise design limitations of the system and allows one to analytically find the optimal f_{sw} and v_{dc}^* in accordance to desired position on the Pareto curve. This provides a clear improvement over the state of the methods that can only evaluate the LC for a fixed design and allows powerful design optimization capability. Possible interesting directions for the future work could be to look at more design parameters or to investigate more complex power electronic systems with unequal stress distributions on its devices.

REFERENCES

[1] F. Blaabjerg, Z. Chen, and S. Kjaer, "Power Electronics as Efficient Interface in Dispersed Power Generation Syst.," *IEEE Trans. on Power Electron.*, vol. 19, pp. 1184–1194, Sept. 2004.

[2] T. Dragicevic, X. Lu, J. C. Vasquez, and J. M. Guerrero, "DC Microgrids-Part II: A Review of Power Architectures, Applications, and Standardization Issues," *IEEE Trans. on Power Electron.*, vol. 31, pp. 3528–3549, May 2016.

[3] V. N. Ferreira, A. F. Cupertino, H. A. Pereira, A. V. Rocha, S. I. Seleme, and B. Cardoso, "Design and selection of high reliability converters for mission critical industrial applications: A rolling mill case study," *IEEE Trans. on Ind. Appl.*, vol. Early Access, pp. 1–10, 2018.

[4] R. Burgos, G. Chen, F. Wang, D. Boroyevich, W. G. Odendaal, and J. D. V. Wyk, "Reliability-oriented design of three-phase power converters for aircraft applications," *IEEE Trans. on Aer. and Electron. Sys.*, vol. 48, pp. 1249–1263, April 2012.

[5] H. Wang, M. Liserre, and F. Blaabjerg, "Toward reliable power electronics: Challenges, design tools, and opportunities," *IEEE Ind. Electron. Mag.*, vol. 7, pp. 17–26, June 2013.

[6] Y. Song and B. Wang, "Survey on reliability of power electronic systems," *IEEE Trans. on Power Electron.*, vol. 28, pp. 591–604, Jan 2013.

[7] M. Musallam, C. Yin, C. Bailey, and M. Johnson, "Mission profile-based reliability design and real-time life consumption estimation in power electronics," *IEEE Trans. on Power Electron.*, vol. 30, pp. 2601–2613, May 2015.

[8] N. C. Sintamarean, F. Blaabjerg, H. Wang, F. Iannuzzo, and P. de Place Rimmen, "Reliability oriented design tool for the new generation of grid connected pv-inverters," *IEEE Trans. on Power Electron.*, vol. 30, pp. 2635–2644, May 2015.

[9] A. Sangwongwanich, Y. Yang, D. Sera, and F. Blaabjerg, "Lifetime evaluation of grid-connected pv inverters considering panel degradation rates and installation sites," *IEEE Trans. on Power Electron.*, vol. 33, pp. 1225–1236, Feb 2018.

[10] D. Zhou, G. Zhang, and F. Blaabjerg, "Optimal selection of power converter in dfig wind turbine with enhanced system-level reliability," *IEEE Trans. on Ind. Appl.*, vol. Early Access, pp. 1–9, 2018.

[11] K. Hornik, M. Stinchcombe, and H. White, "Multilayer feedforward networks are universal approximators," *Neural Networks*, vol. 2, no. 5, pp. 359 – 366, 1989.

[12] M. Liserre, F. Blaabjerg, and S. Hansen, "Design and control of an lcl-filter-based three-phase active rectifier," *IEEE Trans. on Ind. Appl.*, vol. 41, no. 5, pp. 1281–1291, 2005.

[13] J. Muhlethaler, M. Schweizer, R. Blattmann, J. W. Kolar, and A. Ecklebe, "Optimal design of lcl harmonic filters for three-phase pfc rectifiers," *IEEE Trans. on Power Electron.*, vol. 28, pp. 3114–3125, July 2013.

[14] A. Reznik, M. G. Simoes, A. Al-Durra, and S. M. Muyeen, "*lcl* filter design and performance analysis for grid-interconnected systems," *IEEE Trans. on Ind. Appl.*, vol. 50, pp. 1225–1232, March 2014.

[15] D. G. Holmes, T. A. Lipo, B. P. McGrath, and W. Y. Kong, "Optimized design of stationary frame three phase ac current regulators," *IEEE Trans. on Power Electron.*, vol. 24, pp. 2417–2426, Nov 2009.

[16] U. Scheuermann, R. Schmidt, and P. Newman, "Power cycling testing with different load pulse durations," in *7th IET Int. Conf. on Power Electron., Machines and Drives (PEMD 2014)*, pp. 1–6, April 2014.

[17] P. D. Reigosa, H. Wang, Y. Yang, and F. Blaabjerg, "Prediction of bond wire fatigue of igbts in a pv inverter under a long-term operation," *IEEE Trans. on Power Electron.*, vol. 31, pp. 7171–7182, Oct 2016.

[18] J. Schmidhuber, "Deep learning in neural networks: An overview," *Neural Networks*, vol. 61, pp. 85 – 117, 2015.

[19] B. Singh, V. Verma, and J. Solanki, "Neural network-based selective compensation of current quality problems in distribution system," *IEEE Trans. on Ind. Electron.*, vol. 54, pp. 53–60, Feb 2007.

[20] Q.-J. Zhang, K. C. Gupta, and V. K. Devabhaktuni, "Artificial neural networks for rf and microwave design - from theory to practice," *IEEE Trans. Microw. Theory Tech.*, vol. 51, pp. 1339–1350, Apr 2003.

[21] H. Kabir, Y. Wang, M. Yu, and Q. J. Zhang, "Neural network inverse modeling and applications to microwave filter design," *IEEE Trans. Microw. Theory Tech.*, vol. 56, pp. 867–879, April 2008.

[22] D. E. Rumelhart, G. E. Hinton, and R. J. Williams, "Learning representations by back-propagating errors," *Nature*, vol. 323, Oct 1986.